Available online at www.sciencedirect.com
SCIENCE DIRECT®
ELSEVIER
International Journal of Solids and Structures 43 (2006) 2693–2709
INTERNATIONAL JOURNAL OF SOLIDS and STRUCTURES
www.elsevier.com/locate/ijsolstr

The mechanics of pyramids

Paul R. Heyliger *, John Kienholz

Department of Civil Engineering, Colorado State University, Fort Collins, CO 80523, USA

Received 21 January 2005; received in revised form 17 May 2005
Available online 12 September 2005

Abstract

The elastostatic fields and free-vibration characteristics are studied for a class of continuous solids in the shape of homogeneous or layered pentahedral pyramids. The pyramids possess an arbitrary number of linear elastic layers containing dissimilar elastic constants. The layers are assumed to be perfectly bonded in the out-of-plane direction of the pyramid. The change in elastic stiffness across each interface requires a model that allows for a jump in displacement gradient at these location. A discrete-layer representation is used that combines the Ritz method with polynomial in-plane approximations with one-dimensional Lagrangian interpolation polynomials in the thickness direction. The free-vibration characteristics are examined for a variety of isotropic and anisotropic materials and representative bulk stiffness estimates are given for homogeneous pyramids under static deformation.

Keywords: Layers; Pyramids; Vibration; Frequency; Stiffness

1. Introduction

Pyramids are a relatively rare and somewhat neglected class of structure, but encompass a range of well recognized examples such as the very small quantum dot (Bimberg et al., 1999). Studies of the basic mechanics are limited but require a continuum theory for accurate representation, since most simplified models do not directly account for the tapered geometry of these elements. Nearly all previous studies of this class of solid have dealt with either homogeneous pyramids (Visscher et al., 1991; Heyliger et al., 2005) or those involving a truncated pyramid in the form of a skewed parallelepiped (Irie et al., 1987). In this study, estimates are sought for the characteristics associated with free-vibration behavior and the basic force-deformation behavior under static load for homogeneous and layered pyramids. These novel

* Corresponding author. Tel.: +1 970 491 6685; fax: +1 970 491 7727.
E-mail address: prh@engr.colostate.edu (P.R. Heyliger).

0020-7683/$ - see front matter
doi:10.1016/j.ijsolstr.2005.06.103

structures possess interesting features that merit further investigation. This is the objective of the present work.

2. Theory

2.1. Geometry

The basic geometry of a typical pentahedral pyramid is shown in Fig. 1. The base and each layer interface lies in the x–y plane. The thickness dimension coincides with the z-axis. The dimensions of the base in the x- and y-directions are $2d_1$ and $2d_2$, respectively. The origin of the rectangular Cartesian coordinate system is located at the peak of the pyramid and the base is located a distance d_3 away in the z-direction. The distance from the peak to the bottom of layer i is H_i. Having the positive z-direction point "down", as shown in Fig. 1, might be somewhat unconventional, but this definition makes subsequent integrations more efficient. The layers are composed of potentially dissimilar materials with independent mass density and elastic constants. The pyramids are assumed to be represented as a continuum, with perfect bonding between all layers.

2.2. Variational formulation

Exact solutions to governing equations of motion would be difficult given the geometry of this problem. The Ritz method is used to find approximate solutions to their corresponding weak form. This approach allows for approximation functions that yield breaks in the gradients of the three displacements across an interface.

Hamilton's principle for elastic medium is given by (Tiersten, 1969)

$$\delta \int_{t_0}^{t} \mathrm{d}t \int_V \left[\frac{1}{2}\rho \dot{u}_j \dot{u}_j - \frac{1}{2} C_{ijkl}\varepsilon_{ij}\varepsilon_{kl}\right] \mathrm{d}V + \int_{t_0}^{t} \mathrm{d}t \int_S t_k \delta u_k \, \mathrm{d}S + \int_{t_0}^{t} \mathrm{d}t \int_V f_k \delta u_k \, \mathrm{d}V = 0 \tag{1}$$

Here, t denotes time, V the volume of the pyramid, S its bounding surface, t_k the components of the specified surface tractions, f_k are the components of the body force vector, δ is the variational operator, the overdot differentiation with respect to time, u_k are the components of the displacement vector, and ε_{ij} are the components of infinitesimal strain. The symbol C_{ijkl} signifies the components of the fourth-order elastic-stiffness tensor, which can also be expressed in conventional contracted notation ($\sigma_{11} = \sigma_1$,

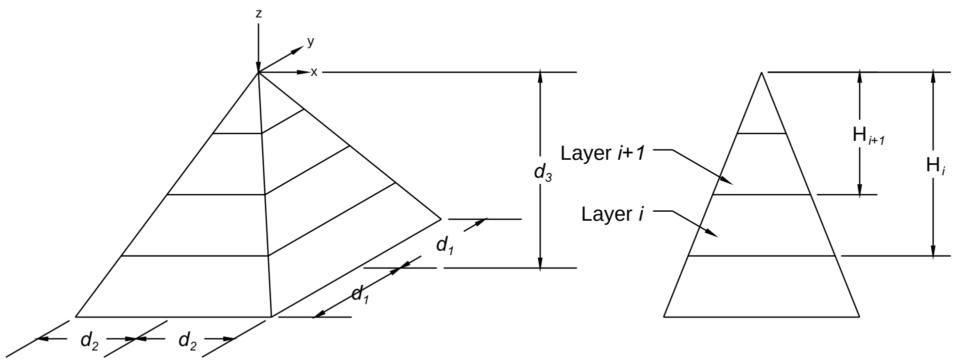

Fig. 1. Geometry and coordinate system for a layered pyramid.

$\sigma_{23} = \sigma_4$, $\varepsilon_{11} = \varepsilon_1$, $2\varepsilon_{23} = \varepsilon_4$, $C_{1111} = C_{11}$, etc.). We assume that each layer is at most orthotropic, with nine independent elastic constants. In contracted notation in terms of the six independent stresses, Hamilton's principle can also be written as

$$0 = -\int_{t_0}^{t}\int_V \{\sigma_1\delta\varepsilon_1 + \sigma_2\delta\varepsilon_2 + \sigma_3\delta\varepsilon_3 + \sigma_4\delta\varepsilon_4 + \sigma_5\delta\varepsilon_5 + \sigma_6\delta\varepsilon_6\}\,\mathrm{d}V + \mathrm{d}t\int_{t_0}^{t}\int_V f_k\delta u_k\,\mathrm{d}V$$
$$+\frac{1}{2}\delta\int_{t_0}^{t}\int_V \rho\left(\dot{u}^2 + \dot{v}^2 + \dot{w}^2\right)\mathrm{d}V\,\mathrm{d}t + \int_{t_0}^{t}\int_S t_k\delta u_k\,\mathrm{d}S\,\mathrm{d}t \tag{2}$$

The constitutive relation for stress and strain for each layer can been expressed as

$$\sigma_{ij} = C_{ijkl}\varepsilon_{kl} \tag{3}$$

and the strain–displacement relations are given as

$$\varepsilon_{ij} = \frac{1}{2}(u_{i,j} + u_{j,i}) \tag{4}$$

The displacement components, $u_1 = u(x,y,z)$, $u_2 = v(x,y,z)$, and $u_3 = w(x,y,z)$, are expressed in terms of the coordinates $x_1 = x$, $x_2 = y$, $x_3 = z$. Substituting the constitutive and strain–displacement relations into Hamilton's principle yields the final weak form of the equations of motion.

2.3. The discrete layer model

Solutions to the weak form of the equations of motion are sought using the Ritz method. The displacements are approximated using a finite linear combinations of a set of basis functions that take the form (Reddy, 1984)

$$\begin{aligned}
u(x,y,z,t) &= \sum_{j=1}^{n} c_j^u \Psi_j^u(x,y,z,t)\\
v(x,y,z,t) &= \sum_{j=1}^{n} c_j^v \Psi_j^v(x,y,z,t)\\
w(x,y,z,t) &= \sum_{j=1}^{n} c_j^w \Psi_j^w(x,y,z,t)
\end{aligned} \tag{5}$$

The parameters c_j are then solved to satisfy Hamilton's principle. Here, Ψ_j denotes the jth approximation functions, which must satisfy the boundary conditions and be continuous as required by the variational principle.

The approximations to the three independent displacements are generated in terms of the global coordinates x, y and z. The layered pyramids considered here possess material properties that are constant in any xy plane but may be discontinuous in the z-direction. They also possess tapered edges. The functions approximating the dependence on the z-coordinate are separated from those for the x- and y-coordinates, and can be expressed in the form

$$\begin{aligned}
u(x,y,z,t) &= \sum_{j=1}^{n} U_j(t)\Gamma_j^u(x,y,z) = \sum_{i=1}^{m}\sum_{j=1}^{n} U_{ji}(t)X_i^u(x,y)Z_j^u(z)\\
v(x,y,z,t) &= \sum_{j=1}^{n} V_j(t)\Gamma_j^v(x,y,z) = \sum_{i=1}^{m}\sum_{j=1}^{n} V_{ji}(t)X_i^v(x,y)Z_j^v(z)\\
w(x,y,z,t) &= \sum_{j=1}^{n} W_j(t)\Gamma_j^w(x,y,z) = \sum_{i=1}^{m}\sum_{j=1}^{n} W_{ji}(t)X_i^w(x,y)Z_j^w(z)
\end{aligned} \tag{6}$$

One-dimensional functions are used for $Z_j(z)$ for each of the three displacement components and there are m in-plane approximation functions. The separation of dependence on time and space for the three displacements is accomplished by making only the layer constants dependent on time. For static problems, these time-dependent functions reduce to a set of unknown constants. There are several different types of basis functions that can be used for the two-dimensional approximation functions $X_i(x,y)$. For this study, power series of the form $x^p y^q$ were used because they are simple to integrate in closed form over a pyramid layer.

A critical feature of the present model is the selection of the linear Lagrangian interpolation polynomials for the approximation of the dependence on the z-coordinate. These functions do not enforce continuity of the derivatives of the functions across a discrete-layer interface, and are far more accurate for pyramids where this interface is between two dissimilar materials. They are piecewise continuous and take the form

$$Z_j(z) = \begin{cases} 0, & \text{for layers} > j \\ \left(\dfrac{z - H_{j+1}}{H_j - H_{j+1}}\right), & \text{for layer } j \\ 1 - \left(\dfrac{z - H_j}{H_{j-1} - H_j}\right), & \text{for layer } j-1 \\ 0, & \text{for layers} < j-1 \end{cases} \tag{7}$$

Here, H_j is the distance from the peak to the bottom of the jth layer. Although higher-order thickness approximations are easily introduced, the results in this study were obtained using linear approximations. With this development of the basis functions, the dependence on the z-direction is separated from the dependence in the x–y plane. From traction continuity there is a break in the gradients of the displacements at an interface between dissimilar materials. By using functions that have discontinuous derivatives located at the interfaces, the break in the slopes of the displacements can be accurately modeled.

For the case of a homogeneous pyramid, the gradients of the displacements will be continuous throughout the pyramid. The model presented here will always have discontinuous gradients at the interface of approximation layers, but will converge to a continuous derivative at interfaces between layers made of the same material. For a pyramid with M layers, there are $M + 1$ interfaces when the base and peak are included. The number of layers used in the Ritz model is equal to or greater than the number of different material layers in the pyramid. The number of layers is only greater when the material layers are themselves divided into sub-layers. We show in the section on results that global basis functions with continuous derivatives are far more accurate than those computed using the one-dimensional Lagrangian polynomials. It is only when the layers are dissimilar is the discrete-layer approach superior.

Substituting the approximations of Eq. (6) into the weak form and placing the results in matrix form yields

$$\omega^2 \begin{bmatrix} [M^{uu}] & [0] & [0] \\ [0] & [M^{vv}] & [0] \\ [0] & [0] & [M^{ww}] \end{bmatrix} \begin{Bmatrix} \overline{u} \\ \overline{v} \\ \overline{w} \end{Bmatrix} + \begin{bmatrix} [K^{uu}] & [K^{uv}] & [K^{uw}] \\ [K^{vu}] & [K^{vv}] & [K^{vw}] \\ [K^{wu}] & [K^{wv}] & [K^{ww}] \end{bmatrix} \begin{Bmatrix} \overline{u} \\ \overline{v} \\ \overline{w} \end{Bmatrix} = \begin{Bmatrix} \overline{f^u} \\ \overline{f^v} \\ \overline{f^w} \end{Bmatrix} \tag{8}$$

The overbars in this expression refer to vectors that contain the numerical value of the specific constant that multiplies each respective term in either the displacement vector or the forcing function. The elements of each of these sub-matrices have forms that preclude preintegration in z, which is often completed in other discrete-layer models (Reddy, 1987; Heyliger et al., 1994). The exact entries for the sub-matrices are given in the Appendix.

One of the appealing features when using approximation functions in the form of power series is that the entries of the mass and stiffness matrices involve only polynomial functions in the three coordinate directions. The integration of the elements over the domain of the pyramid can be completed analytically as (Visscher et al., 1991)

$$\int_V x^p y^q z^r \,\mathrm{d}V = \frac{d_1^{p+1} d_2^{q+1} d_3^{r+1}}{(p+q+r+3)(p+1)(q+1)} \tag{9}$$

The geometry, as discussed in the previous section, was defined with this formula in mind and it allows for integration of a power series over the domain of a pyramid, V, which is defined by d_1, d_2, d_3 and H_i with the origin of z at the pyramid tip.

Each integrand within the mass or stiffness matrix is defined piecewise over individual layers since material properties may change from one layer to the next. This means that the integration over the pyramid's domain must also be completed piecewise over each layer. The integration over layer i is completed by taking the difference between the integration over a domain defined using the ith interface and the integration over a domain defined using the $(i+1)$th interface. Conveniently, all integrals vanish if the power of either x or y is odd.

2.4. Free vibration analysis

One of the key areas of interest in this study is the completely free vibration of a pyramid. In this case, the traction and body force vectors in Hamilton's principle will vanish. Assuming periodic motion, the displacements have the form

$$\begin{aligned} u(x,y,z,t) &= u(x,y,z)\mathrm{e}^{i\omega t} \\ v(x,y,z,t) &= v(x,y,z)\mathrm{e}^{i\omega t} \\ w(x,y,z,t) &= w(x,y,z)\mathrm{e}^{i\omega t} \end{aligned} \tag{10}$$

where ω is the natural frequency. Taking the second derivative with respect to time of these equations gives

$$([K] - \omega^2[M])\{\Delta\} = \{0\} \tag{11}$$

Here, ω is the natural frequency and $\{\Delta\}$ is the eigenvector that contains the constants associated with each approximation function for the specific mode shape. This equation can be solved using standard methods.

2.5. Static analysis

Under static conditions, the inertial terms in the weak form will vanish, and the resulting matrix equation reduces to the solution of a linear system where the load vector is known and the unknowns are the layer constants. The final form of this matrix and its structure depends on the boundary conditions and the forcing function vector, but the overall general matrix form remains the same as that given in Eq. (8) in with $\omega = 0$ and a non-zero right-hand side.

2.6. Group theory

Application of the Ritz method to calculate the static fields, natural frequencies, and mode shapes of layered pyramids can lead to relatively large systems of equations. One of the advantages of the Ritz method compared to more conventional computational methods (most notably finite element approximations) is that the global basis functions provide far more computational efficiency when the domain is continuous and regular. Even so, it is possible and desirable to reduce the size of the linear system or eigenvalue problem using elements of group theory. Using finite elements, this would be the equivalent to the use of symmetry to reduce the size of the modeled domain that requires meshing. The use of group theory in the

Table 1
Groups for power series in x and y

Group	u		v		w	
	x	y	x	y	x	y
1	Even	Even	Odd	Odd	Odd	Even
2	Even	Odd	Odd	Even	Odd	Odd
3	Odd	Even	Even	Odd	Even	Even
4	Odd	Odd	Even	Even	Even	Odd

selection of approximation functions allows for a significant reduction in the size of the system of equations that requires solution. Applications of group theory to problems of vibrating parallelepipeds were first discussed within the context of the vibration of parallelepipeds (Ohno, 1976) which contains details of this general approach. Here, we provide only the fundamental features of how it applies to the layered pyramid, for which the basic principles are the same.

For the pyramids of this study, the x and y axes are lines of physical symmetry. Given that the materials used in this study are assumed to have at most orthotropic symmetry, the pattern of induced deformation can be used to separate any potential motion into one of four groups, each with a very specific type of physical character. Each group has a different set of linearly independent basis functions to approximate the three displacements for each mode that coincide with each type of possible motion. The form of each type of approximation function is given in Table 1. By combining the complete vibrational spectra (or the static deformation response) into displacement approximation functions that include only functions from these groups, the size of the eigenvalue problem (or that of the linear system in the case of static deformation) is roughly one quarter its original size. In all results that follow, this form of symmetry was exploited to the greatest extent possible. This decomposition has no impact on the nature of the results (provided sufficient machine precision is present), but will dramatically reduce computational effort.

3. Results

In this section, results are presented for the natural frequencies and mode shapes for both homogeneous and layered pyramids and the elastic fields under static conditions. There are two objectives to this section: (1) determine the level of accuracy possible given a fixed number of approximation terms and (2) present basic results for the mechanics of homogeneous and layered pyramids.

3.1. Convergence: vibration of homogeneous pyramids

Convergence is studied for the free vibration case as both the number of layers, M, and the highest order of in-plane approximation functions, N, are increased. The value of N controls the number of terms used in the approximation functions where all combinations of $x^p y^q$ are used with

$$N \geqslant p + q \tag{12}$$

The number of degrees-of-freedom for the entire system can be found using

$$D = \frac{3(N+1)(N+2)(M+1)}{2} \tag{13}$$

Here, the value D indicates the total number of degrees-of-freedom and does not incorporate separation of this number into the sum of four small numbers via group theory. Convergence was studied for homogeneous pyramids with three different types of material symmetry—isotropic, cubic, and orthotropic. The frequencies found by the present method are compared with those found by a global Ritz method and/or a finite element approach. Each pyramid will possess six rigid-body modes corresponding to zero frequency. These are recovered in the analysis, but not listed in results that follow.

The global Ritz method (Heyliger et al., 2005) used here for purposes of comparison differs from the method of this study in the sense that it uses full power series in all three Cartesian coordinates to approximate the three independent displacements u, v and w. This ensures that the behavior of the pyramid in the z-direction is modeled differently than that of the global method. The global Ritz method approach will be a better approximation for homogeneous pyramids because its displacement derivatives in z are continuous. The true strength of the method presented here is the ability to model heterogeneous, layered pyramids where the displacement derivatives are not continuous across an interface of dissimilar media. Hence for a given value of D, the global approach yields more accurate values for homogeneous pyramids. However, the method fails when applied to dissimilar media.

The material properties used for each of the three homogeneous cases are given in Table 2. The resulting frequencies have been scaled using

$$\omega_{\text{norm}} = \omega\sqrt{\frac{\rho}{C_{44}}}d_1 \tag{14}$$

These normalized values are given in the results that follow.

The first pyramid studied is homogeneous and isotropic. The material properties used are those in the first column of Table 2. This material has a ratio of Lamé parameters given by $\lambda/\mu = 1.5$ and a pyramid geometry defined by $d_1/d_2 = d_1/d_3 = 1$. The first 20 non-zero frequencies (rad/s) were calculated using one, two, four, eight, 16 and 32 layers and using N from 1 to 11. The percent error E was calculated based on the results of the global Ritz method using up to 10 terms in power series for the three displacements. Fig. 2 shows the maximum percent error of the first 20 frequencies as a function of both M and N. Table 3 shows the results from the global Ritz method along with the results from the present method and their percent difference.

Several features are clear from these results. If a single layer is used and N is increased, the method converges to an over-approximation of the frequencies and cannot get within ten percent of the reference value. Similarly, the method does not yield reasonable accuracy for N less than about five. Fig. 2 shows that for this geometry the method converges faster by increasing the number of in-plane functions than by increasing the number of layers, but both must be increased in order to converge on the results of the global Ritz method. Fig. 2 also shows that the method appears to converge to within 1% for the lowest 20 frequencies using 16 layers and $N = 10$. There is little accuracy gained by going from 16 layers to 32 or by increasing N from 10 to 11.

Table 2
Elastic coefficients for three homogeneous materials used in the numerical examples

Elastic coefficients	Isotropic	(Cubic) GaN (GPa)	(Orthotropic) B–Al (GPa)
C_{11}	3.5	293	189.6
C_{22}	3.5	293	189.6
C_{33}	3.5	293	246.4
C_{12}	1.5	159	95.0
C_{13}	1.5	159	48.0
C_{23}	1.5	159	48.0
C_{44}	1.0	155	57.0
C_{55}	1.0	155	57.0
C_{66}	1.0	155	47.1

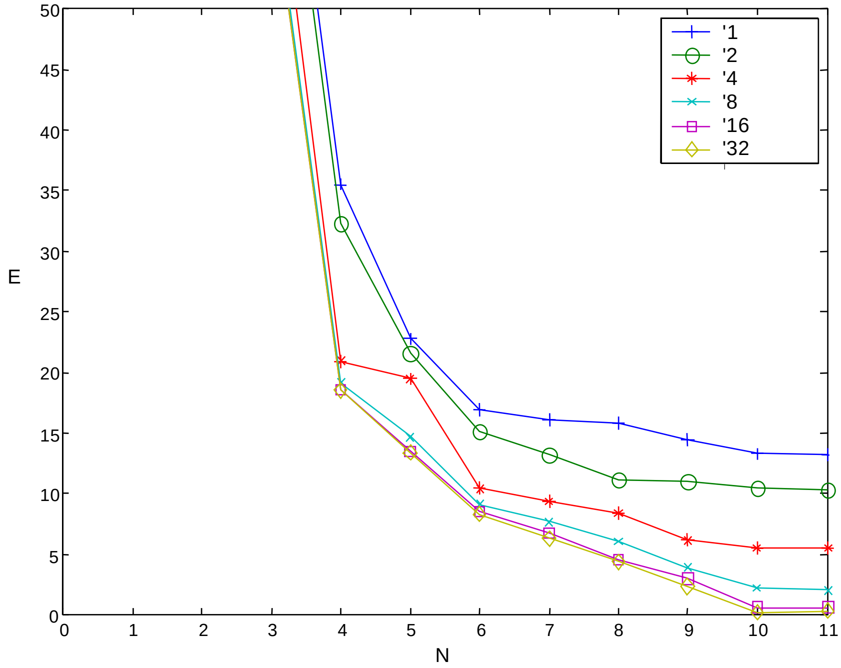

Fig. 2. Convergence of maximum error in frequency for an isotropic pyramid. Each curve represents the error for a varying number of layers through the thickness.

Table 3
Frequencies and percent error for an isotropic pyramid using 16 layers and $N = 10$

Mode	Global Ritz	Discrete-layer Ritz	Percent error (%)
1	1.0687	1.0702	0.14
2	1.5241	1.5260	0.13
3	1.6159	1.6212	0.33
4	1.7660	1.7711	0.29
5	1.7660	1.7711	0.29
6	2.3466	2.3476	0.04
7	2.3466	2.3476	0.04
8	2.5496	2.5617	0.47
9	2.5496	2.5617	0.47
10	2.5935	2.6026	0.35
11	2.6067	2.6176	0.42
12	2.6393	2.6494	0.38
13	2.8252	2.8262	0.04
14	2.8602	2.8688	0.30
15	3.1146	3.1171	0.08
16	3.4514	3.4730	0.62
17	3.4514	3.4730	0.62
18	3.5138	3.5165	0.08
19	3.6217	3.6414	0.54
20	3.6577	3.6782	0.56

A second homogeneous pyramid studied was composed of the cubic material gallium nitride, or GaN. The aspect ratio is identical to the previous example, and the elastic constants were taken from column 2 of

Table 1. Convergence was studied using the same approach as that in the previous section for the homogeneous, isotropic pyramid. The frequencies for the first 20 non-rigid body modes were calculated using 1, 2, 4, 8, 16 and 32 layers and for N's from 1 to 11. The results converge in a fashion similar to that of the isotropic pyramid. The first nonzero frequency converges within 1% using eight layers and $N = 5$ (567 total degrees-of-freedom) and within 1% for the first 20 frequencies using 16 layers and $N = 10$ (3366 total degrees-of-freedom). Numerical results for the lowest 20 frequencies are shown in Table 4. Results are higher than those of the values from the global Ritz model, but most of the lower frequencies yield three-place agreement. Hence 16 layers and terms to order 10 consistently yield accuracy within 1% for isotropic and cubic pyramids.

A third and final homogeneous pyramid was composed of the boron–aluminum, B–Al, which was assumed to be orthotropic. The aspect ratio for this pyramid is defined by $d_1/d_2 = 1$ and $d_3/d_1 = 2$. The elastic constants were taken from Ledbetter et al. (1995) and are given in the third column of Table 1. As with the other homogeneous examples, the first 20 frequencies were calculated while varying the number of layers (1, 2, 4, 8, 16 and 32) and N from 1 to 11. For comparison with this example, a three-dimensional finite element model was constructed using one quarter of the pyramid. The mesh of the pyramid models the positive x- and y-quadrants and used 1496 8-noded brick elements with 1785 nodes. There were a total of 16 divisions used in the x- and y-directions along the flat base of the quadrant, and 16 divisions in the vertical direction of the pyramid. Collapsed elements were used where necessary. Symmetry along $x = 0$ and $y = 0$ was used to represent all vibrational modes of the complete pyramid. Imposition of symmetry yielded four sets of boundary conditions or groups defined as follows: Group 1 ($v(0,y) = w(0,y) = u(x,0) = w(x,0) = 0$), Group 2 ($u(0,y) = v(x,0) = 0$), Group 3 ($u(0,y) = u(x,0) = w(x,0) = 0$) and Group 4 ($v(0,y) = w(0,y) = v(x,0) = 0$). Each of these finite element symmetry groups has an analogous companion in the groupings of the Ritz approximation functions by nature of the orders of the enclosed order of the power series terms (these group numbers may differ, however). The maximum percent error or percent difference is shown for each case in Table 5. In this case, the frequencies are again in very good agreement with the discrete-layer values being the

Table 4
Frequencies and percent error for a GaN pyramid using 16 layers and $N = 10$

Mode	Global Ritz	Discrete-layer Ritz	Percent error (%)
1	0.7112	0.7123	0.16
2	0.7252	0.7263	0.16
3	0.8824	0.8862	0.43
4	1.0540	1.0571	0.30
5	1.0540	1.0571	0.30
6	1.1577	1.1586	0.08
7	1.1577	1.1586	0.08
8	1.2959	1.2967	0.06
9	1.3774	1.3856	0.59
10	1.3774	1.3856	0.59
11	1.4121	1.4178	0.40
12	1.4652	1.4664	0.08
13	1.5287	1.5345	0.38
14	1.6035	1.6159	0.78
15	1.8633	1.8649	0.09
16	1.8633	1.8710	0.41
17	1.8879	1.8894	0.08
18	1.9268	1.9416	0.77
19	1.9673	1.9733	0.30
20	1.9673	1.9733	0.30

Table 5
Frequencies and percent error for a B–Al pyramid using 16 layers and $N = 10$

Mode	FEM	Discrete-layer Ritz	Percent difference (%)
1	1.373	1.369	−0.29
2	1.827	1.818	−0.50
3	2.054	2.046	−0.39
4	2.054	2.046	−0.39
5	2.183	2.170	−0.60
6	2.265	2.255	−0.60
7	2.265	2.255	−0.60
8	2.350	2.339	−0.47
9	2.401	2.384	−0.71
10	2.401	2.384	−0.71
11	2.423	2.418	−0.21
12	2.718	2.713	−0.18
13	2.780	2.771	−0.32
14	3.108	3.090	−0.58
15	3.108	3.090	−0.58
16	3.201	3.175	−0.82
17	3.220	3.177	−1.35
18	3.331	3.287	−1.34
19	3.331	3.287	−1.34
20	3.508	3.461	−1.36

lower and hence more accurate of the two sets of results. We discuss other comparisons between the discrete-layer and finite element representations in the next section.

3.2. Layered pyramids: free vibration

In this section, the free vibration behavior of layered isotropic and anisotropic pyramids are explored. The first example considers a heterogeneous pyramid comprised of two layers of dissimilar isotropic materials. The dimensions of this heterogeneous pyramid are $d_1/d_2 = 1$ and $d_3/d_1 = 2$. The bottom material (from the base to half-height) is defined by setting the Lamé's parameter ratio as $\lambda/\mu = 1.5$. The top material (from half-height to the peak at $z = 0$) uses a fixed value of $\lambda = 1.5$, but the shear modulus is varied with scaled multiples of 1, 2, 5, 10, 20 and 50. The densities are assumed to be identical, and the value of C_{44} in Eq. (14) is that of the lower layer. The estimated frequencies are compared to the solutions from a finite element approach for the shear modulus ratio of 5:1. The intent of this example is to demonstrate the influence of the mismatch in shear modulus.

The convergence study of this heterogeneous case was done in a similar manner as to that completed for the homogeneous cases. The frequencies were found for each case while varying N from one to eleven and the number of layers, 2, 4, 8, 16, and 32 layers. The convergence trends are very similar to those of the previous examples. The results for 10 in-plane terms and 16 layers are shown in Table 6. Several features are clear. First, although excellent agreement exists between the formulations, the results of the present model are significantly more accurate than those of the finite element results. This is especially true for the higher modes, where the difference between formulations begins to exceed one percent. This is a striking difference in frequency given that the finite element model requires 5355 degrees-of-freedom for each group calculation for the pyramid quadrant (the number of active degrees-of-freedom is lessened slightly after imposition of the appropriate boundary conditions, but only by about 10%) compared with 867–765–867–867 degrees-of-freedom for each of the four Ritz groups (the complete approximation represents 66 in-plane terms for

Table 6
Frequencies of a pyramid with 2 layers of dissimilar isotropic materials with the finite element symmetry group number in parentheses

Mode	FEM (Group)	Discrete-layer Ritz	Percent difference (%)
1	1.4967 (1)	1.4900	−0.45
2	1.9348 (2)	1.9212	−0.71
3	2.1445 (2)	2.1304	−0.66
4	2.1757 (3)	2.1663	−0.43
5	2.1757 (4)	2.1663	−0.43
6	2.3587 (3)	2.3414	−0.74
7	2.3587 (4)	2.3414	−0.74
8	2.4963 (1)	2.4833	−0.52
9	2.6800 (3)	2.6562	−0.90
10	2.6800 (4)	2.6562	−0.90
11	2.6725 (1)	2.6654	−0.27
12	2.7962 (2)	2.7892	−0.25
13	2.9990 (2)	2.9855	−0.45
14	3.0579 (2)	3.0382	−0.65
15	3.1501 (3)	3.1304	−0.63
16	3.1501 (4)	3.1304	−0.63
17	3.3471 (1)	3.2915	−1.69
18	3.5578 (2)	3.5201	−1.07
19	3.5743 (3)	3.5262	−1.36
20	3.5743 (4)	3.5262	−1.36

each of the three displacements at 17 layer end-points, or $66 \times 3 \times 17 = 3366$ total degrees-of-freedom divided into the four symmetry groups). Hence this model is both more accurate and far more efficient than a conventional FEM calculation.

Plots of the mode shapes for four different shear moduli ratios are presented in Fig. 3. In these figures, the displacements have been normalized so that the largest displacement takes the value of unity and the pictures of the pyramids show highly exaggerated deformations. The location of most interest is denoted by the arrows in the figures, located at the corner of the interface between the layers. As the level of mismatch in shear modulus increases, the physical kink becomes more pronounced. For the most extreme ratio shown of 10, the softer lower layer undergoes far more deformation than does the upper layer, which in fact begins to take on the appearance of a rigid cap. Fig. 4 further demonstrates this behavior, showing the explicit kink behavior of the u-displacement component along the centerline for the first repeated frequency, and the relative smoothing that occurs as the ratio of shear moduli tends to unity.

In a final example of free vibration, a cross-ply rectangular-base boron–aluminum pyramid is studied. The half-length in the x-direction is 5 and the half-length in the y-direction is 1. The peak-to-base dimension is 1. The interface between the two layers is located halfway between the base and the peak. For each layer of the pyramid, the fibers are oriented in the xy-plane, but the second layer is rotated 90° (about the z-axis) from the first. There are two lamination schemes studied. Pyramid 1 has the fibers oriented in the long or x-direction in the bottom layer of the laminate, and the top layer has fibers oriented in the short or y-direction. Pyramid 2 reverses this lamination scheme. Its bottom layer has its fibers oriented in the short direction and the top layer has the fibers in the long direction. The elastic constants for each layer is given in Table 7.

The frequencies and mode shapes for the first five modes of these two pyramids were found and compared as shown in Fig. 5. The frequencies associated with Pyramid 1 are higher than those of Pyramid 2 by roughly ten percent. This is to be expected because the bottom layer of Pyramid 1 has the fibers oriented in the longer direction, making this pyramid more resistant to bending about the shorter (y) axis. However,

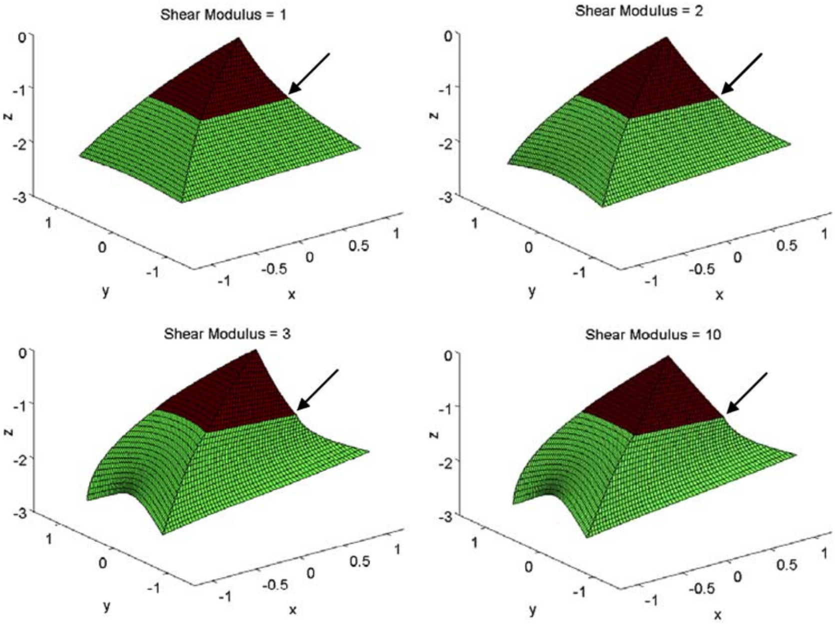

Fig. 3. Representative mode shapes for the layered isotropic bi-material pyramid. The break in slope at the corner of each material layer becomes more distinct as the mismatch in shear moduli increases. The shear modulus ratio between the upper and lower levels varies from 1 to 10.

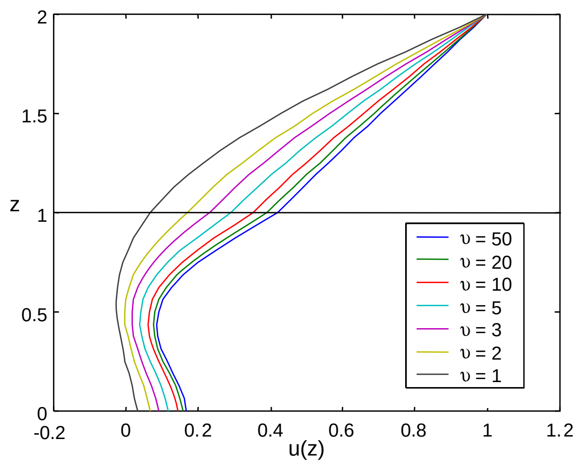

Fig. 4. The through-thickness plot of the x-component of displacement for the layered isotropic bi-material pyramid. As the shear modulus mismatch increases, the break in slope across the interface becomes more pronounced, and demonstrates why single-layer theories or those with continuous derivatives across an interface will be less accurate. The shear modulus ratio is denoted as υ in this figure.

this is a significant change from a rectangular cross-ply plate, which would have the same frequency regardless of lamination scheme. This figure also shows that the third and fourth mode shapes have switched

Table 7
Rotated elastic constants of B–Al

Elastic constants	Fibers in the x-direction (long)	Fibers in the y-direction (short)
C11	246.4	189.6
C22	189.6	246.4
C33	189.6	189.6
C12	48.0	48.0
C13	48.0	95.0
C23	95.0	48.0
C44	47.1	57.0
C55	57.0	47.1
C66	57.0	57.0

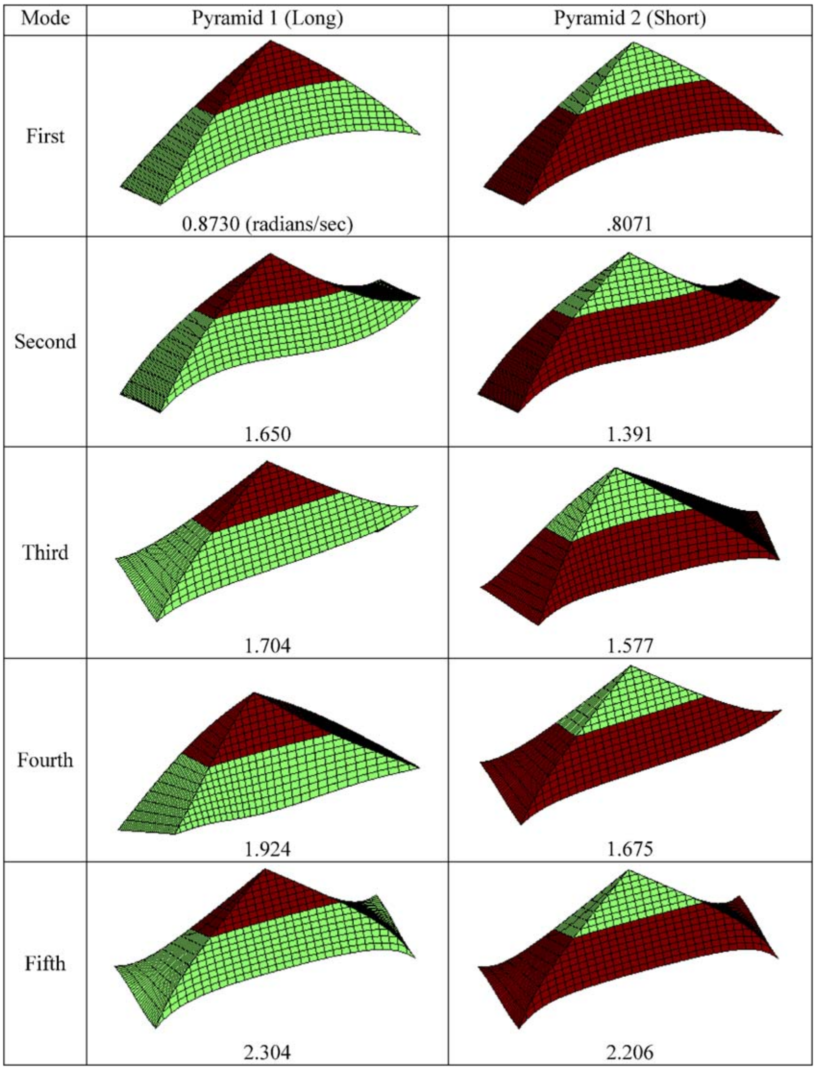

Fig. 5. The modal shapes for the cross-ply orthotropic pyramid. The pyramids on the left possess a lower layer with fibers in the long direction. Note the change in deformation pattern between modes 3 and 4.

sequential order when the lamination scheme is reversed, indicating a change in physical dependence on layer material properties. In material characterization studies, this type of dependence could be used to construct a pyramid specimen to isolate specific elastic constants and their influence on natural frequency spectra, or to eliminate the degenerate frequencies that are independent of lamination scheme.

3.3. Static response

The overall bulk stiffness of a given pyramid can be approximated by examining the force–displacement relationship for a pyramid under point load at the tip. This is of importance for several reasons, including the use of triangular geometries for certain types of probes or sensors. We focus on isotropic and homogeneous pyramids with equal volume but differing geometries that are subjected to a unit point load at the peak in the vertical or horizontal direction. The initial quantities of interest are the displacements along the vertical line underneath the applied load. Pyramids were selected with a square base and a total volume of 8/3 m^3. The material parameters were $\lambda = 1.5$ GPa and $\mu = 1.0$ GPa. Five square pyramids were selected with varying height/half-length (H/d_1) ratios: $0.088(0.25/\sqrt{8})$, 0.25 (0.5/2), $0.71(1/\sqrt{2})$, 2 (2/1), and $3.7(3/\sqrt{2/3})$. The vertical displacements along the base of the pyramid were fixed at zero. Body weight was neglected. This problem was modeled with the symmetry group that maintains symmetric deformation about the x and y axes with 10 terms and 16 layers through the thickness.

The peak values of downward displacement at the tip for the five cases were, respectively (in nm) as the height/half-length ratio increases, 1.7, 3.1, 5.5, 13.1, and 26.2. In Fig. 6, the variation of this displacement over the height of the pyramid is shown for the five cases. For the taller, thinner pyramids, a significant (over 90%) portion of the deformation takes place in only about 20% of the pyramid height. As the base of the pyramid broadens, this behavior tends to become more linear and in fact reaches a point where the upper regions of the pyramid contribute to proportionally less downward deformation. Also of note is the nature of the deformation over a cross-section with constant z. There is typically very large variation of w over the x–y plane for a given z and it is far from constant (the same is also true for the stress components).

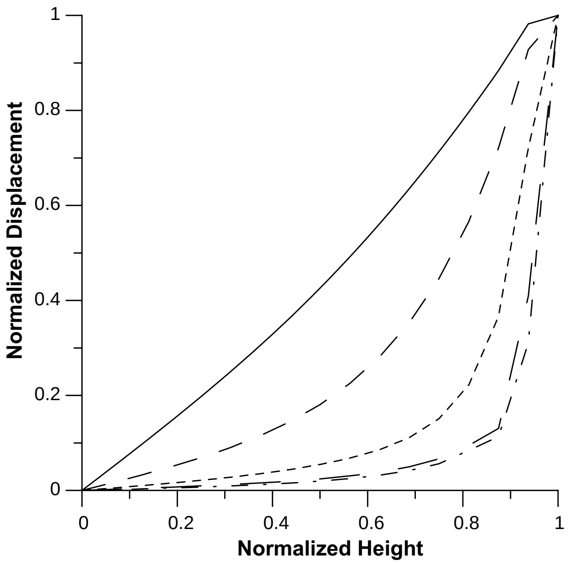

Fig. 6. The normalized through thickness vertical displacement for a unit vertical point load as a function of normalized height. The five curves represent increasing H/d_1 ratio moving from left to right.

For example, for the case of $H/d_1 = 0.71$, the vertical deflection under the line of the load near the tip is about ten times the value at the outer edge of the cross-section. This difference gradually decreases to a factor of about 3 near the base. This variation changes with H/d_1, but it is clear that assumptions such as constant stress over a cross-section must be used with extreme caution. The bulk stiffness of each pyramid is

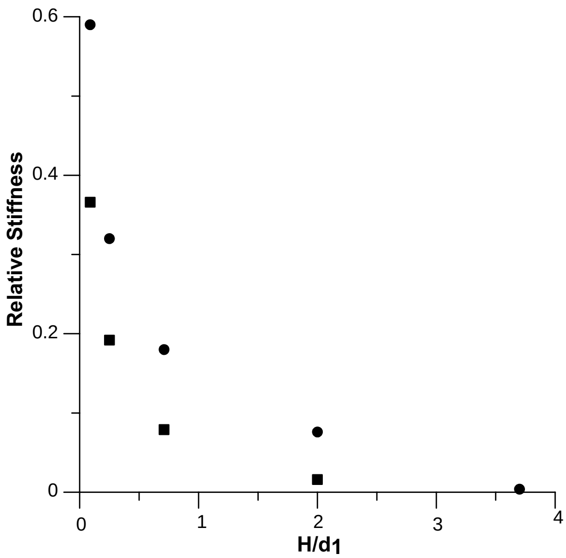

Fig. 7. The effective bulk axial (●) and bending (■) stiffness for pyramids with varying H/d_1 ratio. The stiffness is characterized as the inverse of the maximum displacement for pyramids of equal volume.

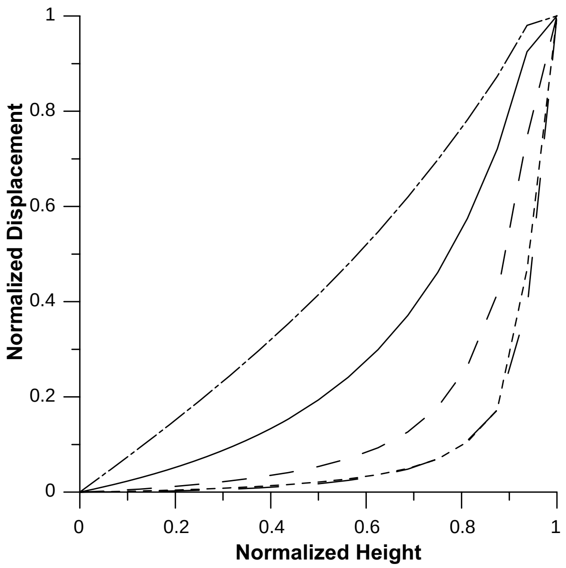

Fig. 8. The normalized through thickness horizontal displacement for a unit horizontal point load as a function of normalized height. The five curves represent increasing H/d_1 ratio moving from left to right.

quantified by the circular points in Fig. 7 (where the effective stiffness is simply the inverse of the maximum displacement for the case of a unit tip load). The stiffnesses are plotted against H/d_1 for each of the five cases (shown as dark circles), and the precipitous decline clearly reinforces the low stiffness/high flexibility of pyramids with H/d_1 ratios approximately greater than 2–3.

A similar analysis was repeated for a horizontal loading at the tip. In Fig. 8, the deformation pattern for the displacement component u at the pyramid centerline is shown for a unit load in the x-direction. However, in this case the aspect ratios of the pyramids studied were slightly modified since the higher values of H/d_1 showed little change in normalized behavior. The results for the pyramid with the aspect ratio of $3.7(3/\sqrt{2/3})$ are not shown, and instead we include a shorter, broader pyramid with ratio of 0.03125 (0.125/4). The results show that for H/d_1 ratios above a value of about one, the upper 10% of the pyramid experiences greater than 80% of the deformation. As the aspect ratio drops, the displacement pattern tends to a more linear variation through the thickness, simulating a much stronger pure-shear type of deformation pattern with the exception of the behavior near the tip. On the plots, this is partly an artifact of our model and the limited number of layers used. The bulk bending stiffnesses for each aspect ratio are shown as plotted squares in Fig. 7 and show the expected drop compared with axial stiffness, although the non-linear trend with H/d_1 is similar.

4. Conclusions

A discrete-layer continuum model was used to study the basic free vibration and static response of homogenous and layered isotropic and orthotropic continuum pyramids. Based on the representative examples included in this study, we summarize our key findings and observations as follows:

1. The discrete layer model developed in this study yields equivalent and slightly better accuracy than finite element models that use over six times the number of degrees-of-freedom. Representative results are provided for a wide variety of examples that yield about three digits in accuracy with 16 layers and terms to order 10 in a power series approximation yielding frequencies within 1%.
2. Under free vibration, the number of degenerate frequencies are far lower than for spheres and parallelepipeds. It is not uncommon for the lowest few modes to be distinct (the first three modes possess this behavior for the isotropic and cubic pyramids studied here), and for the lowest 20 frequencies to include only four repeated pairs. This trait can be exploited to isolate frequencies in characterizing new materials using ultrasonic resonance methods.
3. Based on static deformation response, pyramids with a H/d_1 ratio in excess of about 1 have nearly 80% of their tip flexibility under axial and flexural load linked to the upper 20% of the pyramid. Probe elements could exploit this inherent flexibility and tailor the behavior to match axial and flexural characteristics.

The model presented here has a great deal of accuracy and simplicity, and can be used for many other fields of interest with pyramid structures. Additional features of pyramid mechanics await further exploration.

Appendix A

The specific expressions of the submatrices of Eq. (8) using the middle approximation functions of Eq. (6) are given below, with i and j denoting the respective discrete-layer approximation numbers.

$$M_{ij}^{uu} = \int_V (\rho \Gamma_i^u \Gamma_j^u) \, \mathrm{d}V \tag{A.1}$$

$$M_{ij}^{vv} = \int_V (\rho \Gamma_i^v \Gamma_j^v) \, \mathrm{d}V \tag{A.2}$$

$$M_{ij}^{ww} = \int_V (\rho \Gamma_i^w \Gamma_j^w) \, \mathrm{d}V \tag{A.3}$$

$$K_{ij}^{uu} = \int_V \left(C_{11} \frac{\partial \Gamma_i^u}{\partial x} \frac{\partial \Gamma_j^u}{\partial x} + C_{55} \frac{\partial \Gamma_i^u}{\partial z} \frac{\partial \Gamma_j^u}{\partial z} + C_{66} \frac{\partial \Gamma_i^u}{\partial y} \frac{\partial \Gamma_j^u}{\partial y} \right) \mathrm{d}V \tag{A.4}$$

$$K_{ij}^{uv} = K_{ji}^{vu} = \int_V \left(C_{12} \frac{\partial \Gamma_i^u}{\partial x} \frac{\partial \Gamma_j^v}{\partial y} + C_{66} \frac{\partial \Gamma_i^u}{\partial y} \frac{\partial \Gamma_j^v}{\partial x} \right) \mathrm{d}V \tag{A.5}$$

$$K_{ij}^{uw} = K_{ji}^{wu} = \int_V \left(C_{13} \frac{\partial \Gamma_i^u}{\partial x} \frac{\partial \Gamma_j^w}{\partial z} + C_{55} \frac{\partial \Gamma_i^u}{\partial z} \frac{\partial \Gamma_j^w}{\partial x} \right) \mathrm{d}V \tag{A.6}$$

$$K_{ij}^{vv} = \int_V \left(C_{22} \frac{\partial \Gamma_i^v}{\partial y} \frac{\partial \Gamma_j^v}{\partial y} + C_{44} \frac{\partial \Gamma_i^v}{\partial z} \frac{\partial \Gamma_j^v}{\partial z} + C_{66} \frac{\partial \Gamma_i^v}{\partial x} \frac{\partial \Gamma_j^v}{\partial x} \right) \mathrm{d}V \tag{A.7}$$

$$K_{ij}^{vw} = K_{ji}^{wv} = \int_V \left(C_{23} \frac{\partial \Gamma_i^v}{\partial y} \frac{\partial \Gamma_j^w}{\partial z} + C_{44} \frac{\partial \Gamma_i^v}{\partial z} \frac{\partial \Gamma_j^w}{\partial y} \right) \mathrm{d}V \tag{A.8}$$

$$K_{ij}^{ww} = \int_V \left(C_{33} \frac{\partial \Gamma_i^w}{\partial z} \frac{\partial \Gamma_j^w}{\partial z} + C_{44} \frac{\partial \Gamma_i^w}{\partial y} \frac{\partial \Gamma_j^w}{\partial y} + C_{55} \frac{\partial \Gamma_i^w}{\partial x} \frac{\partial \Gamma_j^w}{\partial x} \right) \mathrm{d}V \tag{A.9}$$

References

Bimberg, D., Grundmann, M., Ledentsov, N.N., 1999. Quantum Dot Heterostructures. Wiley, New York.

Heyliger, P.R., Pan, E., Cook, S., Manaloto, M., 2005. Acoustic modes of anisotropic quantum dots, submitted for publication.

Heyliger, P.R., Ramirez, G., Saravanos, D.A., 1994. Coupled discrete-layer models for laminated piezoelectric plates. Communications in Numerical Methods in Engineering 10, 971–981.

Irie, T., Yamada, G., Tagawa, Y., 1987. Three-dimensional vibration analysis of a truncated quadrangular pyramid. ASME Journal of Applied Mechanics 54, 115–120.

Ledbetter, H., Fortunko, C., Heyliger, P.R., 1995. Orthotropic elastic constants of a B/Al fiber-reinforced composite: an ultrasonic-resonance-spectroscopy study. Journal of Applied Physics 78, 1542–1546.

Ohno, I., 1976. Free vibration of a rectangular parallelepiped crystal and its application to determination of elastic constants of orthorhombic crystals. Journal of the Physics of the Earth 24, 355–379.

Tiersten, H.F., 1969. Linear Piezoelectric Plate Vibrations. Plenum Press, New York.

Reddy, J.N., 1984. Energy and Variational Methods in Applied Mechanics. Wiley, New York.

Reddy, J.N., 1987. A generalization of displacement-based laminate theories. Communications in Applied Numerical Methods 3, 173–181.

Visscher, W.M., Migliori, A., Bell, T.M., Reinert, R.A., 1991. On the normal modes of free vibration of inhomogeneous and anisotropic elastic objects. Journal of the Acoustical Society of America 90, 2154–2162.